Chinese Chemical Letters 36 (2025) 109931

Contents lists available at ScienceDirect

Chinese Chemical Letters

journal homepage: www.elsevier.com/locate/cclet

Effects of nanosized Au on the interface of zinc phthalocyanine/TiO_2 for CO_2 photoreduction

Linlu Bai[a,1,*], Wensen Li[a,b,1], Xiaoyu Chu[a,b], Haochun Yin[a], Yang Qu[a], Ekaterina Kozlova[c], Zhao-Di Yang[b], Liqiang Jing[a,*]

[a] Department Key Laboratory of Functional Inorganic Materials Chemistry (Heilongjiang University), Ministry of Education, School of Chemistry and Materials Science, International Joint Research Center and Lab for Catalytic Technology, Harbin 150080, China
[b] School of Materials Science and Chemical Engineering, Harbin University of Science and Technology, Harbin 150080, China
[c] Federal Research Center Boreskov Institute of Catalysis, 630090 Novosibirsk, Russian Federation

ARTICLE INFO

Article history:
Received 16 December 2022
Revised 31 March 2024
Accepted 27 April 2024
Available online 29 April 2024

Keywords:
Supported MPc photocatalyst
Au nanoparticle
Interface modulation
Charge separation
CO_2 photoreduction

ABSTRACT

The interface modulation significantly affects the photocatalytic performances of supported metal phthalocyanines (MPc)-based systems. Herein, ZnPc was loaded on nanosized Au-modified TiO_2 nanosheets (Au-T) to obtain wide-spectrum ZnPc/Au-T photocatalysts. Compared with large Au NP (8 nm)-mediated ZnPc/Au-T photocatalyst, ultrasmall Au NP (3 nm)-mediated one shows advantageous photoactivity, achieving 3- and 10-fold CO_2 conversion rates compared with reference ZnPc/T and pristine TiO_2 nanosheets, respectively. Employing monochromatic beam-assisted surface photovoltage and photocurrent action, *etc.*, the introduction of ultrasmall Au NPs more effectively facilitates intrinsic interfacial charge transfer. Moreover, ZnPc molecules are found more dispersed with the existence of small Au NPs hence exposing abundant Zn^{2+} sites as the catalytic center for CO_2 reduction. This work provides a feasible design strategy and renewed recognition for supported MPc-based photocatalyst systems.

Carbon neutralization has become a worldwide consensus for addressing the energetic and environmental problems caused by excessive CO_2 content. Among various targeting technologies, photocatalytic CO_2 conversion by utilizing green and sustainable solar energy to produce fuel molecules shows great potential and hence has attracted extensive research interests [1-3]. The key to realizing highly efficient photoconversion of CO_2 depends on the rational design of the photocatalyst.

Titanium oxide (TiO_2) is one of the most investigated and promising semiconductor photocatalysts since the year of 1972, which has been applied to types of environmental and energetic reactions including CO_2 reduction [4-6]. Nevertheless, due to the recombination of charge carriers and lack of catalytic sites, single TiO_2 is not ideal enough in terms of photoactivity and product selectivity. Accordingly, coupling TiO_2 with a suitable semiconductor that contains catalytic sites to obtain heterojunction could improve the charge separation and catalytic efficiency and hence is found to be a feasible strategy [7-11].

Recently, organic molecular semiconductors such as metal phthalocyanines (MPcs) become popular candidates, which are organic heterolytic molecules with a large 18-electron conjugated system [12,13]. Due to the visible-light absorption in the range of 550–800 nm, they are priorly exploited as photosensitizers in the heterojunction systems. What is neglected is that MPc possesses the highest occupied molecular orbital (HOMO) and lowest unoccupied molecular orbital (LUMO) and hence can function as an organic molecular semiconductor to compose heterojunctions photocatalysts [14]. More importantly, MPc contains defined single M-N_4 sites like Zn, Co, Fe, and Ni centers, *etc.*, capable of activating different reactants as catalytic centers [15]. Considering the activation and reduction of CO_2 would significantly influence the photocatalytic CO_2 reduction, hence among typical phthalocyanines, ZnPc has been reported to demonstrate favorable CO_2 activation ability [16,17]. Therefore, coupling ZnPc with TiO_2 might enhance the photoactivity of individual TiO_2. Noteworthily, the interface between ZnPc and TiO_2 shows a significant influence on the charge transfer efficiency hence affecting the photoactivity [18,19]. Therefore, modulating the interface aiming at increasing the conductivity of heterojunction could further enhance the photoactivity.

It is natural to consider introducing metal nanoparticles (NP) such as Au NPs capable of effectively transferring electrons at the

* Corresponding authors.
E-mail addresses: llbai@hlju.edu.cn (L. Bai), jinglg@hlju.edu.cn (L. Jing).
[1] These authors contributed equally to this work.

https://doi.org/10.1016/j.cclet.2024.109931
1001-8417/

interface [20,21]. Especially, the Au NPs with different sizes might show different modulating effects. Moreover, for reported works on Au NP-MPc hybrid materials, it is found with the existence of Au the light absorption of MPc could be extended [22], implying that Au might induce a high dispersion of supported MPc molecules, resulting in high MPc loading amount, a large number of exposed light-absorbing units, short charge transfer distance and most importantly abundant single M-N_4 sites. Therefore, Au-modulated MPc/TiO_2 is feasible and the modulating effects of Au for the charge transfer are worthy of exploration.

In this work, we first synthesized ultrathin TiO_2 nanosheets by F ion-induced assembly method [23], denoted as T for short, which were then decorated by Au NPs using the deposition-precipitation method to obtain Au-T [24]. Subsequently, ZnPc was loaded on Au-T by the H-bond interaction process, resulting in a series of two-dimensional ZnPc/Au-T heterojunction photocatalysts [25]. By contrast with large Au nanoparticles NPs (*ca.* 8 nm), small Au NPs (*ca.* 3 nm) show an advantageous modulating effect. Corresponding optimal ZnPc/Au-T photocatalyst demonstrated 3- and 10-fold CO_2 conversion rates compared with reference ZnPc/T and pristine TiO_2 nanosheets, respectively. The monochromatic beam-assisted surface photovoltage and photocurrent action, *etc.*, the introduction of small Au NPs more effectively facilitates intrinsic interfacial charge transfer. Moreover, ZnPc molecules are found more dispersed with the existence of small Au NPs hence exposing abundant Zn^{2+}sites as a catalytic centers for CO_2 reduction. This work diversifies the strategies for modulating the interface of supported MPc-based nanomaterials.

Ultrathin TiO_2 nanosheets, denoted as T for short in the following passage, were synthesized by solvothermal method with hydrofluoric acid as an additive [23]. ZnPc assemblies were then loaded on the T by self-assembly process to obtain ZnPc/T heterojunctions. To improve the interface between ZnPc and T, Au NPs were deposited on T surface by the deposition-precipitation (DP) method to acquire Au-T samples [24]. Noteworthily, the particle size of Au could be enlarged by post-calcination. The powder X-ray diffraction (XRD) pattern demonstrates the monoclinic phase (JCPDS No. 21-1272) of T (Fig. S1 in Supporting information) [26]. No extra diffraction peaks were observed for representative 1Au-T, 2.5ZnPc/T, and 2.5ZnPc/1Au-T samples compared with T (the number in the sample name indicates the mass ratio relative to T), due to limited loading amounts and relative dispersed state of supported Au NPs and ZnPc assemblies. The morphology of typical samples was examined by transmission electron microscopy (TEM). T shows the ultrathin lamellar structure with a length of 38–80 nm and a width of 35–44 nm (Fig. S2a in Supporting information). For 2.5ZnPc/T, blurring, and dark shadows can be observed on the T surface, which is ascribed to ZnPc assemblies (Fig. S2b in Supporting information). By contrast, the shadows for 2.5ZnPc/1Au-T become lighter, hinting at more dispersed dispersion of ZnPc assemblies when Au NPs (*ca.* 3 nm) exist (Fig. 1a). It is noted when relatively large (*ca.* 8 nm) Au NPs deposited, similar dispersing effect still can be observed for 2.5ZnPc/1Au (L)-T (Fig. 1a inset). The atomic force microscopy (AFM) assured the average thickness of two-dimensional T to be 3.2 nm (Fig. S3 in Supporting information). Compared with T, the thickness increments of 2.5ZnPc/T, 2.5ZnPc/1Au-T and 2.5ZnPc/1Au (L)-T are 1.9, 1.0 and 1.3 nm, respectively (Figs. 1b and c, Fig. S3 in Supporting information). This further proves the introduction of small Au NPs leads to a higher dispersion of ZnPc assemblies. The optical absorption of different samples was analyzed using UV diffuse reflectance (DRS) spectroscopy (Fig. 1d).

The absorption edge of T is around 400 nm due to the vacancies. The absorption peaks at around 520 nm are observed for 1Au-T and 1Au (L)-T, owing to the surface plasmon resonance (SPR) effect of Au [27]. Notably, the peak for 1Au-T is broader due to smaller particle sizes. It is inferred that calcination temperature and the size of Au nanoparticles size influence the activity of the plasma reaction [28]. For ZnPc/T, the extended light absorption in the range of 500–800 nm is attributed to ZnPc assemblies [16]. Interestingly, the light absorption for 2.5ZnPc/1Au (L)-T and especially 2.5ZnPc/1Au-T is more extended, corresponding to a higher dispersion of ZnPc assemblies assured by AFM results.

To investigate the effect of Au on the interface of the heterojunctions, the Fourier transform infrared spectra (FT-IR) and X-ray photoelectron spectroscopy (XPS) were collected (Figs. 1e and f, Fig. S4 in Supporting information). For the FTIR spectra, all samples possess the band at 500 cm^{-1} attributed to the O–Ti–O bond of TiO_2 [29]. For 2.5ZnPc/T, the bands at 1288 and 1485 cm^{-1} originate from the stretching vibration of the C=N bond and the bending vibration of the C–H bond belonging to ZnPc, respectively [29]. Noteworthily, compared with that for 2.5ZnPc/T, the bands due to the C–N= bond both shift to larger wavelength for 2.5ZnPc/1Au-T and 2.5ZnPc/1Au (L)-T. The slightly larger shift for 2.5ZnPc/1Au-T shreds of evidence stronger interaction between small Au NPs and ZnPc than the situation for 2.5ZnPc/1Au (L)-T, which is responsible

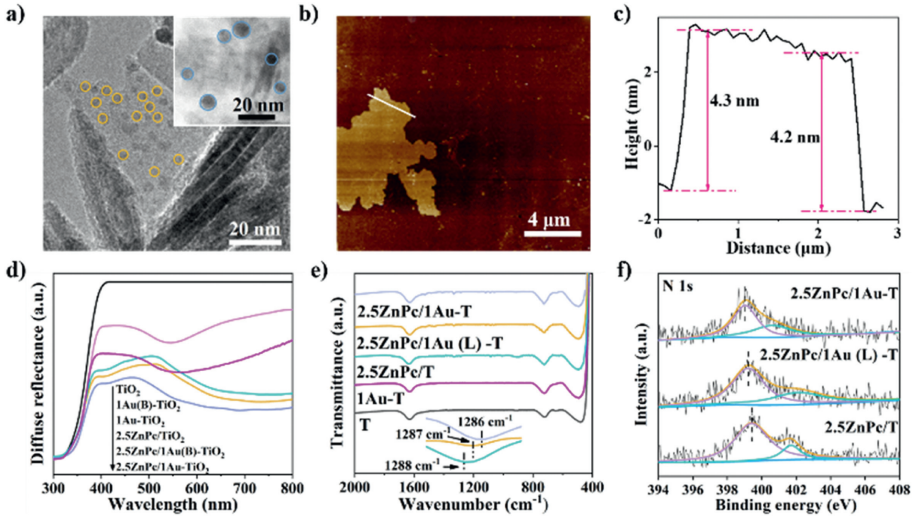

Fig. 1. (a) TEM image of 2.5ZnPc/1Au-T and 2.5ZnPc/1Au (L)-T (inset). (b, c) AFM image and the corresponding height profiles of 2.5ZnPc/1Au-T. (d) DRS spectra, (e) FT-IR spectra, and (f) XPS N 1s spectra of different samples.

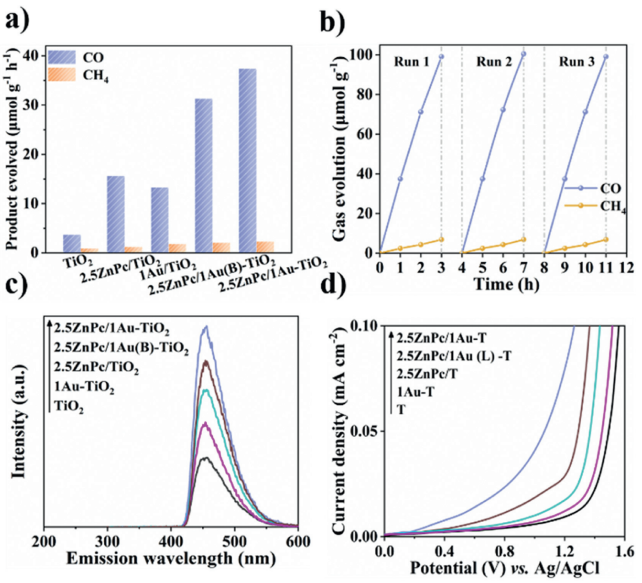

Fig. 2. (a) Photoactivities of T, 2.5ZnPc/T, 1Au-T, 2.5ZnPc/1Au (L)-T and 2.5ZnPc/1Au-T for CO_2 reduction. (b) Three consecutive runs of CO_2 conversion by 2.5ZnPc/1Au-T. (c) Fluorescence spectra related to the formed hydroxyl radicals. (d) Photoelectrochemical *I-V* curves.

for the dispersing effect of Au for ZnPc assemblies. Moreover, in the N 1s XPS spectra, compared with the N 1s peaks of 2.5ZnPc/T, the ones for 2.5ZnPc/1Au-T and 2.5ZnPc/1Au (L)-T shifted to the lower binding energies, confirming the interaction between Au NPs and the N atoms of ZnPc macrocycles in agreement with the FT-IR results [30]. This is consistent with the reported interaction between the macrocycles of MPc and underlying metallic states [22].

The photocatalytic performances of as-fabricated heterojunctions were tested for CO_2 reduction performance under UV–vis light irradiation. As shown in Fig. S5a, as the loading amount of ZnPc increases, 2.5ZnPc/T shows the largest CO_2 conversion rate of 15.6 μmol h^{-1} g^{-1}, with CO and CH_4 as products. Furthermore, by alternatively adjusting the amounts of Au and ZnPc, the best sample 2.5ZnPc/1Au-T was obtained (Fig. S5b), providing the 3- and 10-fold CO_2 conversion rate of 2.5ZnPc/T and T, respectively (Fig. 2a). It is noted that small Au NPs show more obvious improving effect on the photoactivity than large ones. Considering that stability is another important indicator to evaluate the performance of the photocatalyst, the three consecutive runs were conducted over 2.5ZnPc/1Au-T. As shown in Fig. 2b, the photocatalytic performance is maintained in each run, evidencing the favorable stability of 2.5ZnPc/1Au-T photocatalysts under reaction conditions. To explore the photocatalytic mechanism, the charge separation as the key factor determining photoactivity was investigated by several classic techniques.

Generally, the FS related to produced hydroxyl radicals under illumination could reflect the charge separation of photocatalysts [17]. Therefore, the FS signals were collected and shown in Fig. 2c and Fig. S6 (Supporting information). The signal intensities follow the order of T < 1Au/T < 2.5ZnPc/T < 2.5ZnPc/1Au-T. Compared with pristine T, the construction of 2.5ZnPc/T heterojunction effectively improves the charge separation. Furthermore, with Au introduced 2.5ZnPc/1Au-T demonstrates the strongest signal intensity among all ternary samples, especially which is stronger than that for 2.5ZnPc/1Au (L)-T. It is found the charge separation of samples indicated by FS results well corresponds with the photo activities. The introduction of Au NPs, especially small ones, greatly improves charge separation. Besides, the linear scanning voltammetry curves of different samples under UV–vis irradiation show that the photocurrent densities increase in the same order as FS signal intensities (Fig. 2d). Additionally, the Electrochemical Impedance Spectroscopy (EIS) of different samples indicates 2.5ZnPc/1Au-T has the smallest curve radius among all samples indicating the best charge separation (Fig. S7 in Supporting information). To conclude, small Au NPs-mediation greatly improves the charge transfer between ZnPc and T hence enhancing the photoactivity. This might be attributed to the conductivity of Au NPs and shortened charge transfer distance due to Au-mediated higher dispersion of supported ZnPc assemblies.

As above, the general charge separation situation of typical samples has been verified, however, the specific charge transfer mechanism of Au-mediated ZnPc/T heterojunction is worthy of in-depth exploration. For MPc/semiconductor photocatalytic systems, MPc is commonly recognized to function as the photosensitizer. The electrons of such heterojunctions would transfer from excited MPc to the semiconductor then induce reduction reactions. Nevertheless, it is always neglected that ZnPc possesses intrinsic HOMO (*ca.* −1.5 eV) and LUMO (*ca.* 0.5 eV), which can function as an organic reduction semiconductor [16]. As assured conduction band (−0.87 eV) and valance band (2.27 eV) of T by the Mott-Schottky curves combining DRS results (Fig. S8 in Supporting information), ZnPc and T might possibly compose Z-scheme heterojunction, resulting in electron transfer from T to ZnPc. Accordingly, to verify the specific charge separation mechanism, tailored investigating techniques including single-wavelength-assisted steady-state surface photovoltage spectroscopy (SPS) and monochromatic photocurrent action spectra (MPAS) were conducted in the atmosphere of N_2 to exclude the influence of oxygen-capturing electron. The SPS spectra of different samples are shown in Fig. 3a. A single 660 nm auxiliary light was added to ensure the simultaneous excitation of ZnPc and T under a single wave scan to verify the Z-scheme charge transfer mechanism. It can be seen that the pure T basically shows no SPS response in the atmosphere of N_2. The obvious signal was observed for 1Au-T, due to electron transfer from T to Au NPs as electron capturer. A stronger SPS signal was recorded for 2.5ZnPc/T from 300 nm to 400 nm with an additional 660 nm monochromatic excitation beam, indicating effective charge transfer from T to ZnPc obeying Z-scheme when both ZnPc and T were excited. Notably, the SPS signal of 2.5ZnPc/1Au/T heterojunction from 300 nm to 400 nm is much stronger than that of 2.5ZnPc/T, again proving ultrasmall Au NPs facilitate the Z-scheme charge transfer from T to ZnPc.

The Z-scheme charge transfer mechanism was further verified by the monochromatic photocurrent action spectra (MPAS) in Fig. 3b. For pristine T, the photocurrent responses were only detected with the excitation wavelength of 350 and 370 nm in the UV region, which are ascribed to the threshold wavelength of T. For 2.5ZnPc/T, identical photocurrent responses to those of pris-

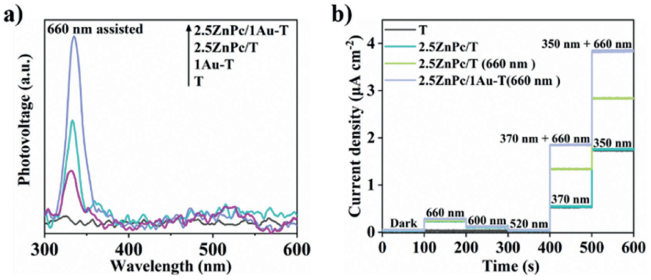

Fig. 3. (a) SPS responses of T, 1Au-T, 2.5ZnPc/T and 2.5ZnPc/1Au-T under an N_2 atmosphere with the assistance of a 660 nm monochromatic beam. (b) MPAS of T, 2.5ZnPc/T, 2.5ZnPc/T (660 nm assisted) and 2.5ZnPc/1Au-T, respectively.

tine T were observed with the same excitation wavelength at 350 and 370 nm. This indicates when only T was excited, no electron transfer occurred for 2.5ZnPc/T. What is different, a small response appeared with the excitation wavelength of 660 nm capable of exciting ZnPc, corresponding to the photosensitization charge transfer mechanism, or rather the electron transfer from ZnPc to T. The limited response indicates that although the photosensitization mechanism exists, however, which only results in weak charge separation. Interestingly, when the 660 nm monochromatic light is introduced as an assistant excitation light source for ZnPc, an apparent response increase could be found for 2.5ZnPc/T with the excitation wavelength at 370 and 350 nm. This firmly indicates when both ZnPc and T were excited, the electrons would transfer from T to ZnPc, evidencing the Z-scheme charge transfer mechanism. With the same assistant 660 nm monochromatic light, the responses of 2.5ZnPc/1Au-T further increase with the excitation wavelength of 370 and 350 nm compared with those of 2.5ZnPc/T, proving the positive effect of Au NPs on Z-scheme charge transfer from T to ZnPc. These findings are in good agreement with the single-wavelength SPS results, highlighting the dominant charge transfer mechanism for 2.5ZnPc/T and 2.5/1Au-T be the Z-scheme instead of photosensitization. In addition, the photoactivity of 2.5ZnPc/1Au-T was acquired under different combinations of monochromatic light (Fig. S9 in Supporting information). When simultaneously using 365 and 660 nm light, the photoactivity reaches the maximum, which is advantageous over the photoactivity using either 365 nm light or 660 nm light. This indicates only when ZnPc and T were both excited, the charge transfer to the largest extent could be reached, in consequence of best photoactivity. The above results support the conclusion that the charge transfer of 2.5ZnPc/1Au-T dominantly obeys the Z-scheme mechanism.

Except for the light absorption and charge separation, catalytic efficiency is another factor significantly affecting photoactivity. To explore the catalytic function of as-fabricated samples, the electrochemical reduction curves (EC) with atmosphere control were collected on different samples. With N_2 and CO_2 bubbled into the test system, the EC curves were demonstrated in Figs. 4a and b for comparison. It is found that only for 2.5ZnPc/T and 2.5ZnPc/1Au-T the onset potentials obviously decrease, indicating that ZnPc plays a vital role in the catalytic CO_2 reduction. This is consistent with the design strategy of introducing ZnPc containing single and precise Zn-N_4 as favorable catalytic sites for CO_2 reduction. Of note, with the existence of Au NPs, 2.5ZnPc/1Au-T shows a smaller onset potential compared with 2.5ZnPc/T. It is concluded that Au-mediated high dispersion of ZnPc would lead to abundant Zn-N_4 sites to benefit the catalytic CO_2 reduction. Basing all above, the introduction of ultrasmall Au NPs in the 2.5ZnPc/1Au-T heterojunction not only extends the visible-light absorption but effectively facilitates the Z-scheme charge transfer and promotes the catalytic function for CO_2 reduction, which comprehensively contribute to the favorable photocatalytic performance for CO_2 reduction.

To further reveal the catalytic process mechanism, the reaction intermediates were investigated by *in situ* FTIR mimicking the photocatalytic reaction conditions (Fig. 4c). The active species including m-CO_3^{2-} (1374, 1508 cm^{-1}), HCO_3^- (1456, 1488 and 1645 cm^{-1}), COOH* (1541 cm^{-1}) and *CO (2017 cm^{-1}) were detected for T, 2.5ZnPc/T and 2.5ZnPc/1Au-T, which are involved in the conversion process from CO_2 to CO as the main product [31,32]. Obviously, for the same duration, the peaks of key intermediates for 2.5ZnPc/1Au-TiO_2 show the largest intensities, consistent with the best photoactivity. According to the *in situ* FTIR results, it is speculated that during the CO_2 conversion process the adsorbed CO_2 turns to COOH* then produces CO.

Based on the above experimental results and analysis, the whole photocatalytic process mechanism over ZnPc/Au-T was proposed as Scheme 1. Under UV–vis irradiation, ZnPc and T are simultaneously excited and the photogenerated electrons transfer from the conduction band of T to Au NPs and then combine with the holes of ZnPc conforming to the Z-scheme charge separation mechanism. Based on Au-improved charge separation, the holes of T would induce water oxidation while the photoelectrons would reduce activated CO_2 by Zn(II)-N_4 centers. In addition, the design strategy for ZnPc/Au-T photocatalyst is found applicable for other transition-metal MPcs (M = Ni, Co and Fe). It can be seen in Fig. S10 (Supporting information) when loading identical amounts of MPcs, 2.5ZnPc/Au-T against the grain demonstrates the best photocatalytic performance.

In conclusion, by introducing small Au NPs with a diameter of *ca.* 3 nm between ZnPc and T nanosheets, the ZnPc/Au-T heterojunctions were successfully synthesized. For photocatalytic CO_2 reduction, optimized 2.5ZnPc/1Au-T demonstrates 3- and 10-fold photoactivity enhancement compared with 2.5ZnPc/T and pristine T, respectively, with CO and CH_4 as products. Advantageous over large Au NPs (8 nm), small ones more effectively facilitated the Z-scheme charge transfer from T to ZnPc, supported by FS, SPS and MAPS results. Moreover, the interaction between Au NPs and the aromatic ring of ZnPc proved by FTIR and XPS resulted in higher dispersion of ZnPc assemblies hence extending the visible-light adsorption meanwhile exposing abundant Zn-N_4 catalytic sites. This

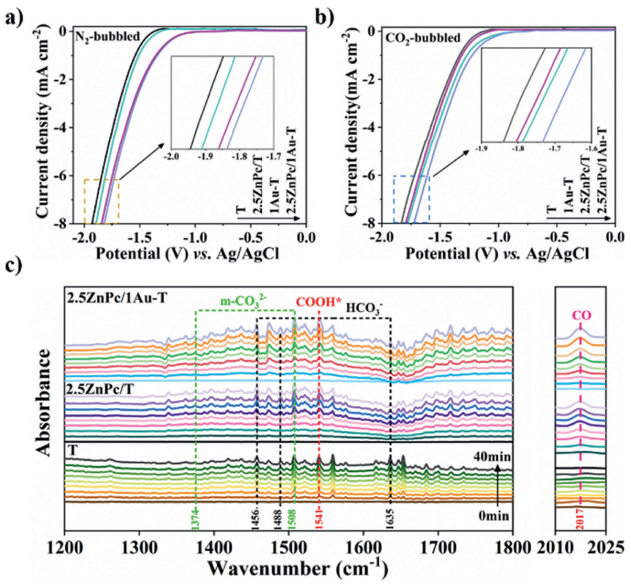

Fig. 4. (a) EC reduction curves in N_2-bubbled and (b) CO_2-bubbled systems, respectively. (c) *In situ* FTIR spectra of T, 2.5ZnPc/T and 2.5ZnPc/1Au-T for the photocatalytic CO_2 reduction.

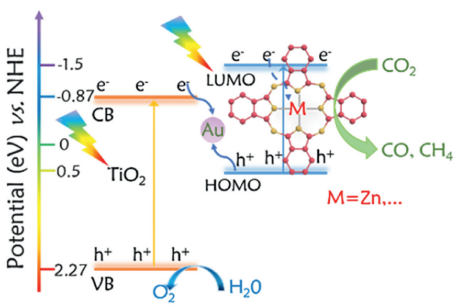

Scheme 1. Schematic of photocatalytic mechanism over ZnPc/Au-T photocatalyst for CO_2 reduction.

work provides a new strategy to design MPc-involved heterojunctions for efficient solar-to-fuel conversion.

Declaration of competing interest

The authors declare that they have no known competing financial interests or personal relationships that could have appeared to influence the work reported in this paper.

CRediT authorship contribution statement

Linlu Bai: Conceptualization, Data curation, Formal analysis, Funding acquisition, Investigation, Methodology, Project administration, Supervision, Validation, Writing – review & editing. **Wensen Li:** Data curation, Formal analysis, Investigation, Methodology, Resources, Software, Validation, Visualization, Writing – original draft. **Xiaoyu Chu:** Methodology, Validation. **Haochun Yin:** Formal analysis, Validation. **Yang Qu:** Validation. **Ekaterina Kozlova:** Validation. **Zhao-Di Yang:** Validation, Formal analysis. **Liqiang Jing:** Conceptualization, Funding acquisition, Validation.

Acknowledgments

This work was supported by the National Natural Science Foundation of China (Nos. U2102211 and 22378101), and the Fundamental Research Foundation for Universities of Heilongjiang Province (No. 2021-KYYWF-0004). Thanks to the Science Fund for Distinguished Young Scholars of Heilongjiang University (No. JCL202102).

Supplementary materials

Supplementary material associated with this article can be found, in the online version, at doi:10.1016/j.cclet.2024.109931.

References

[1] C.A. Trickett, A. Helal, B.A. Al-Maythalony, et al., Nat. Rev. Mater. 2 (2017) 17045–17060.
[2] D.U. Nielsen, X.M. Hu, K. Daasbjerg, T. Skrydstrup, Nat. Catal. 2 (2018) 95.
[3] Y.F. Li, Y.C. Wei, Z.L. Tang, et al., Chin. Chem. Lett. 34 (2023) 108417.
[4] L. Jiang, S. Zhou, J. Yang, et al., Adv. Funct. Mater. 32 (2021) 2108977.
[5] Q.S. Zhang, X. Yang, Y. Liu, et al., Chin. Chem. Lett. 34 (2023) 107628.
[6] R. Schappi, D. Rutz, F. Dahler, et al., Nature 601 (2022) 63–68.
[7] Z. Xiong, H. Wang, N. Xu, et al., Int. J. Hydrog. Energy 40 (2015) 10049–10062.
[8] Z. Xiong, Z. Lei, Y. Li, L. Dong, Y. Zhao, J. Zhan, J. Photochem. 36 (2018) 24–47.
[9] J. Wang, R.T. Guo, Z.X. Bi, X. Chen, X. Hu, W.G. Pan, Nanoscale 14 (2022) 11512–11528.
[10] F. Xu, K. Meng, B. Cheng, et al., Nat. Commun. 11 (2020) 4613–4621.
[11] T. Zhang, X. Han, N.T. Nguyen, L. Yang, X. Zhou, Chin. J. Catal. 43 (2022) 2500–2529.
[12] J. Fernandez-Ariza, R.M. Krick Calderon, M.S. Rodriguez-Morgade, D.M. Guldi, T. Torres, J. Am. Chem. Soc. 138 (2016) 12963–12974.
[13] A. de la Escosura, M.V. Martinez-Diaz, P. Thordarson, et al., J. Am. Chem. Soc. 125 (2003) 12300–12308.
[14] D. Chen, K. Wang, W. Hong, et al., Appl. Catal. B 166-167 (2015) 366–373.
[15] Y.Y. Wang, Y. Qu, B.H. Qu, et al., Adv. Mater. 33 (2021) 2105482.
[16] J. Bian, J. Feng, Z. Zhang, et al., Angew. Chem. Int. Ed. 58 (2019) 10873–10878.
[17] J. Bian, J. Feng, Z. Zhang, et al., Chem. Commun. 56 (2020) 4926–4929.
[18] L. Wang, W. Chen, D. Zhang, et al., Chem. Soc. Rev. 48 (2019) 5310–5349.
[19] S.D. Sun, L.P. He, M. Yang, J. Cui, S.H. Liang, Adv. Funct. Mater. 32 (2021) 2106982.
[20] M. Wang, Q.T. Han, L. Li, et al., Nanotechnology 28 (2017) 274002.
[21] N. Zhang, S. Xie, B. Weng, Y.J. Xu, J. Mater. Chem. A 4 (2016) 18804–18814.
[22] P. Khurana, S. Thatai, N.B. Chaure, S. Mahamuni, S. Kulkarni, Thin Solid Films 565 (2014) 202–206.
[23] Z. Wang, J. Feng, X. Li, et al., Colloid Interface Sci. 588 (2021) 787–794.
[24] H. Lu, Y. Qu, L. Sun, et al., ACS Sustain. Chem. Eng. 6 (2018) 14652–14659.
[25] J.N. Feng, J. Bian, L.L. Bai, et al., Appl. Catal. B 295 (2021) 120260.
[26] X. Han, Q. Kuang, M. Jin, Z. Xie, L. Zheng, J. Am. Chem. Soc. 131 (2009) 3152–3153.
[27] M. Du, D. Sun, H. Yang, et al., Phys. Chem. C 118 (2014) 19150–19157.
[28] D. Tsukamoto, Y. Shiraishi, Y. Sugano, et al., J. Am. Chem. Soc. 134 (2012) 6309–6315.
[29] Q. Wang, W. Wu, J. Chen, G, et al., Colloids Surf. 409 (2012) 118–125.
[30] P. Gargiani, M. Angelucci, C. Mariani, M.G. Betti, Phys. Rev. B 81 (2010) 085412.
[31] Y.B. Shi, G.M. Zhan, H. Li, et al., Adv. Mater. 33 (2021) 2100143.
[32] K. Wang, M.Y. Cao, J.B. Lu, et al., Appl. Catal. B 296 (2021) 120341.